Novel Core–Shell Structured Mn–Fe/MnO 2 Magnetic Nanoparticles for Enhanced Pb(II) Removal from Aqueous Solution

ARTICLE *in* INDUSTRIAL & ENGINEERING CHEMISTRY RESEARCH · DECEMBER 2014

Impact Factor: 2.59 · DOI: 10.1021/ie502967a

6 AUTHORS, INCLUDING:

Hua Zhang

Chinese Academy of Sciences

20 PUBLICATIONS **255** CITATIONS

SEE PROFILE

Gaosheng Zhang

Chinese Academy of Sciences

38 PUBLICATIONS **1,322** CITATIONS

SEE PROFILE

I&EC research
Industrial & Engineering Chemistry Research

Article

pubs.acs.org/IECR

Novel Core–Shell Structured Mn–Fe/MnO_2 Magnetic Nanoparticles for Enhanced Pb(II) Removal from Aqueous Solution

Jing Chen,[†,‡] Faming He,[†,‡] Hua Zhang,[†] Xiaolei Zhang,[§] Gaosheng Zhang,*[,†,‡] and Guodong Yuan[†]

[†]Key Laboratory of Coastal Environmental Processes and Ecological Remediation and [‡]Shandong Provincial Key Laboratory of Coastal Environmental Processes, Yantai Institute of Coastal Zone Research (YIC), Chinese Academy of Sciences (CAS), Shandong 264003, China

[§]Environment and Material Engineering College, Yantai University, Shandong, 264005, China

ABSTRACT: Lead (Pb) is a priority pollutant, and the demand is growing for its cost-effective removal from water. A nanomaterial with Mn(II)-bearing Fe_3O_4 (Mn–Fe) as magnetic core and MnO_2 as shell was synthesized, giving a specific surface area of 113.3 m^2/g, particle size of 90–130 nm, cubic spinel magnetic phase, and saturation magnetization of 35.1 emu/g. It exhibited a strong propensity for adsorbing Pb(II), with a maximal adsorption capacity of 261.1 mg/g at pH 5.0. The process was rapid and pH dependent, but only slightly affected by ionic strength and coexisting cations, indicating the formation of the inner-sphere complexes. Used nanomaterial could be easily separated from solution by a magnet and readily regenerated with HCl. Its Pb(II) adsorption efficiency remained at about 80% of the original after the fourth regeneration. Thus, it has the potential for use as an effective adsorbent to remove Pb(II) from water.

1. INTRODUCTION

Heavy metals in water are of growing environmental and health concerns because of their high toxicity, persistence in the environment, and tendency for bioaccumulation.[1] Pb has been released from a wide range of industries from plating and mining to ceramics-, glass-, and battery-manufacturing.[1,2] To minimize its health risks (e.g., adverse impact on human nervous system[3]) U.S. EPA regulates the allowable Pb concentration in drinking water to 0.015 mg/L, with zero concentration as a public goal.[4] To this end, a wide range of technologies have been tested for Pb removal. With the advantages of low cost, wide applicability, easy design and operation, adsorption is considered superior to chemical precipitation, membrane filtration, ion exchange, electrochemical treatment, microbe separation, and flotation.[1,5] Among many adsorbents reported for heavy metal removal from water, metal oxides have seen increased applications.[6,7] Recently their uses have been further enhanced with the development of nanosized metal oxides to provide a large surface area and abundant adsorptive sites.[8,9]

Manganese oxides have a strong affinity for heavy metal ions,[10,11] and many have reported the potential of MnO_2 as an adsorbent of Pb(II), Zn(II), Cu(II), and Cd(II).[12−15] Its use in a wastewater treatment plant, however, often requires energy intensive filtration to separate the adsorbent from the aquatic system, which would add the overall cost and cause the blockage of filters.

Magnetic separation is faster and more effective than traditional filtration for separating suspended particles. Its use can improve operation efficiency and reduce overall cost in water/wastewater treatment.[16,17] Furthermore, core–shell structured adsorbents with a magnetically responsive core and a functional shell have the combined advantages of magnetic separation and good adsorption capacity.[18] For example, Wang et al. developed an amino-functionalized Fe_3O_4/SiO_2 core–shell nanoadsorbent, which exhibited good magnetic property and high adsorption affinity for Cu(II), Pb(II), and Cd(II).[19] Warner et al. showed that introduction of manganese dopant to Fe_3O_4 nanoparticles largely increased their chemical affinity and adsorption capacity for heavy metals (i.e., Co, Ni, Zn, As, Ag, Cd, Hg, and TI) when compared to the native oxide material.[20] In our laboratory, a core–shell structured Fe_3O_4/MnO_2 magnetic nanoadsorbent was previously prepared and found to have relatively high adsorption capacity toward Pb(II).[21]

To further enhance Pb(II) removal, it is necessary to develop new adsorbents which can more effectively adsorb Pb(II) and be easily separated from aqueous solution using a magnetic technique. It is proposed that partial substitution of Fe^{2+} by Mn^{2+} in the Fe_3O_4 lattice would form magnetic nanoparticles of Mn(II)-bearing Fe_3O_4 (denoted as Mn–Fe). Coating them with MnO_2 would make a novel core–shell structured adsorbent (denoted as Mn–Fe/MnO_2). Substitution of Fe^{2+} by Mn^{2+} might also increase core–shell affinity and increase adsorption for heavy metals. To our best knowledge, no efforts have been made to fabricate Mn–Fe/MnO_2 magnetic nanoparticles for heavy metal removal from aqueous solution. Here, a novel core–shell structured Mn–Fe/MnO_2 magnetic adsorbent was developed and characterized with multiple techniques. The Pb(II) adsorption behaviors and reusability were investigated to highlight the potential to use it as an effective adsorbent to remove Pb(II) from water.

2. MATERIALS AND METHODS

2.1. Synthesis of Adsorbent. The magnetic core Mn(II)-bearing Fe_3O_4 (Mn–Fe) nanoparticles were prepared accord-

Received: July 25, 2014
Revised: November 5, 2014
Accepted: November 7, 2014
Published: November 7, 2014

dx.doi.org/10.1021/ie502967a | *Ind. Eng. Chem. Res.* 2014, 53, 18481−18488

ing to a modified coprecipitation method of Kodama et al.[22] Briefly, $FeCl_3 \cdot 6H_2O$ was dissolved in deionized water and heated to 60 °C, and appropriate amounts of $MnCl_2 \cdot 4H_2O$ and $FeCl_2 \cdot 4H_2O$ were dissolved in the $FeCl_3$ solution to give a $Mn(II)/Fe_{total}$ molar ratio of 0.3. A solution of 5% polyethylene glycol (PEG) was then added to the metal chloride solution and mixed by ultrasonic stirring. Further, 2 mol/L NaOH solution was added dropwise to the mixed solution at 60 °C with stirring for coprecipitation until the pH reached about 11. The precipitate was aged in the mother liquor at 60 °C for 1 h, separated, washed until Cl^- free, and dried at 60 °C for use in the next step.

A 1.0 g sample of the obtained Mn−Fe particles was dispersed in 5% PEG solution by ultrasonic stirring for 30 min, and then 120 mL of $MnSO_4$ solution of 0.036 mol/L was added to this mixture. After the mixture was heated to 60 °C, 80 mL of $KMnO_4$ solution of 0.036 mol/L was added with stirring to form Mn−Fe/MnO_2 particles, which were magnetically separated, washed with deionized water, and dried at 60 °C for 24 h for use in characterization and adsorption experiments.

2.2. Characterization. X-ray powder diffraction (XRD) patterns of Mn−Fe and Mn−Fe/MnO_2 particles were taken on a D/Max 2500VPC diffractometer with Cu Kα radiation 40 kV and 200 mA. The microscopic morphologies of the synthesized Mn−Fe and Mn−Fe/MnO_2 particles were observed by using a transmission electron microscope (TEM, Hitachi H-800). Specific saturation magnetization (σs), a measure of the particles' magnetism, was determined by a VSM model Lakeshore 7307 magnetic meter at room temperature. Specific surface area (SSA), pore volume, and pore size distribution were determined by nitrogen adsorption−desorption isotherm using the BET method with a Quantachrome Asiq surface area analyzer. The chemical state of elements in samples was determined by X-ray photoelectron spectroscopy (XPS, Thermo VG ESCALAB 250), using Al Kα as an exciting X-ray source (1486.6 eV). C 1s photoelectron peak was used for calibration and fixed at binding energy (BE) equal to 284.6 eV.

2.3. Batch Adsorption and Desorption Experiments. Batch adsorption experiments were conducted to determine the adsorption isotherm, kinetics, and the effects of pH, ionic strength, and coexisting cations on Pb adsorption. Briefly, 25.0 mg of adsorbent was added to a series of 100 mL vessels containing 50 mL of solution of 5−350 mg/L Pb (as $Pb(NO_3)_2$). $NaNO_3$ (0.01 M) was used as the background electrolyte. The vessels were placed on an orbital shaker at 170 rpm for 24 h at 25 ± 1 °C. Solution pH was adjusted to 5.0 ± 0.1 by dilute HCl and/or NaOH solution. At the end of shaking, all suspensions were filtered through 0.45 μm and analyzed for Pb concentration by inductively coupled plasma optical emission spectroscopy (ICP-OES) (Optima 7000 DV, PerkinElmer Co.).

Adsorption kinetics was assessed by adding 0.500 g of Mn−Fe or Mn−Fe/MnO_2 adsorbent to a 2-L glass vessel with 1000 mL of solution of 100 mg/L Pb. The suspension was stirred, and its pH was maintained at 5.0 ± 0.1 throughout the experiment by adding dilute HCl and/or NaOH solution. A 5-mL aliquot was taken from the vessel at specified time intervals and immediately filtered through 0.45 μm for the analysis of Pb by ICP-OES.

To investigate the effect of pH and ionic strength on Pb(II) adsorption, batch experiments were performed at pH values between 2.0 and 7.5 and with 0.001, 0.01, or 0.1 M $NaNO_3$ as background electrolyte. The pH of the solution was adjusted every 4 h to a designated value and the final equilibrium pH was measured. The effect of coexisting cations Ca(II), Mg(II), Cu(II), and Zn(II) on Pb(II) adsorption was assessed by batch experiments at pH 5.0 ± 0.1, with the initial Pb(II) concentration of 50 mg/L, and varying amounts of coexisting cations from 0.025 to 2.5 mM.

Four successive cycles of adsorption and desorption of Pb(II) were carried out in a batch system to evaluate the reusability of prepared Mn−Fe/MnO_2. In the adsorption test, 2.00 g of Mn−Fe/MnO_2 was added into a vessel containing 2 L of solution with 100 mg/L Pb(II). The suspension was stirred for 8 h, and its pH was maintained at 5.0 ± 0.1. At the end, the adsorbent was separated from the suspension and the equilibrium Pb(II) concentration was measured by ICP-OES. In the desorption test, the Pb(II)-containing Mn−Fe/MnO_2 was added into 100 mL of 0.1 M HCl. After the mixture was stirred for 1 h the adsorbent was regenerated, separated from the solution, washed until Cl^- free, and dried for use in the next adsorption−desorption cycle.

3. RESULTS AND DISCUSSION

3.1. Structure, Morphology, Surface Properties, And Saturation Magnetization of As-Synthesized Samples. The crystalline structures of the Mn−Fe and Mn−Fe/MnO_2 nanoparticles were identified with XRD (Figure 1). Diffraction

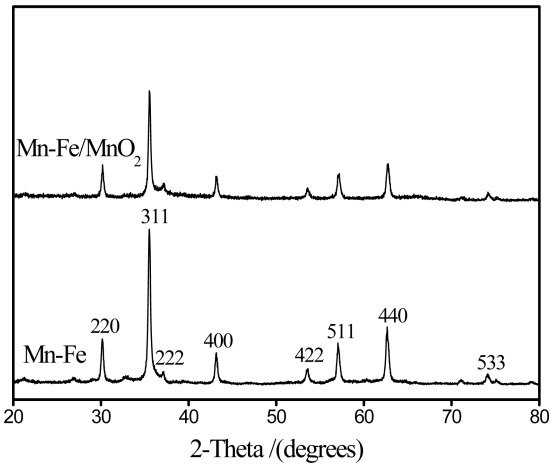

Figure 1. X-ray diffraction patterns of Mn−Fe and Mn−Fe/MnO_2.

peaks of Mn−Fe sample at 2θ = 30.2, 35.5, 37.1, 43.2, 53.6, 57.1, 62.6 and 74.1 are well indexed to the crystal plane of cubic spinel ferrite structure (220), (311), (222), (400), (422), (511), (440), and (533), respectively (JCPDS Card No. 771545). This suggests that the presence of Mn(II) in the magnetic core has little effect on the cubic spinel magnetic phase compared with the presence of pure Fe_3O_4. The XRD pattern of Mn−Fe/MnO_2 showed no obvious crystalline peak other than those of the Mn−Fe core. Thus, the MnO_2 shell is amorphous in nature. The shell made the characteristic peaks less intensive in Mn−Fe/MnO_2 than in Mn−Fe, which is in agreement with the reports of core−shell constructed nanoparticles of Fe_3O_4/MnO_2 and Fe_3O_4/SiO_2-NH_2.[19,21,22] It also made the crystallite size of Mn−Fe/MnO_2 (24.3 nm), estimated from the Scherrer equation, larger than that of Mn−Fe (21.6 nm).

The morphologies of the Mn−Fe core and the Mn−Fe/MnO_2 particles were investigated by transmission electron

dx.doi.org/10.1021/ie502967a | Ind. Eng. Chem. Res. 2014, 53, 18481−18488

microscopy (TEM). In its TEM micrograph the Mn−Fe core appeared as quasi-spherical aggregates, formed by smaller primary nanocrystalline particles (Figure 2a). After being

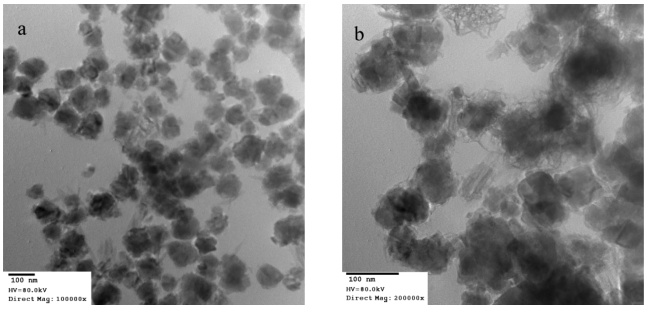

Figure 2. TEM micrographs of (a) Mn−Fe and (b) Mn−Fe/MnO_2.

coated with MnO_2, these aggregates were surrounded by loose floccule, which was attributable to the presence of amorphous MnO_2 (Figure 2b). Thus, it could be deduced that the Mn−Fe/MnO_2 was composed of the crystalline Mn−Fe core and the amorphous MnO_2 shell, which was consistent with the XRD results. The core−shell structure of Mn−Fe/MnO_2 was similar to the structure of Fe_3O_4/SiO_2 and Fe_3O_4/SiO_2−NH_2.[19]

The shell−core structure of Mn−Fe/MnO_2 was also evidenced in XPS spectra (Figure 3). The BE of Mn $2p_{3/2}$

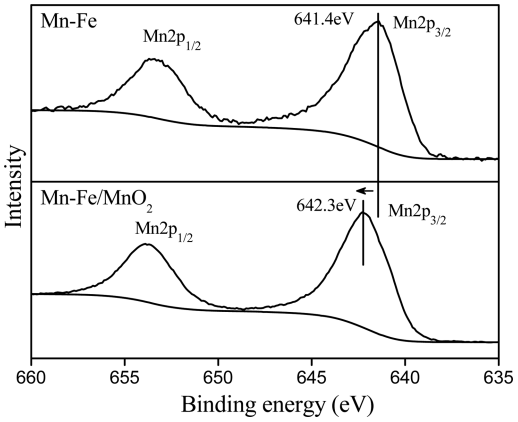

Figure 3. Mn 2p core level photoelectron spectra of Mn−Fe and Mn−Fe/MnO_2.

was 641.4 eV in Mn−Fe core. After it was coated with MnO_2 the value shifted to 642.3 eV and Mn $2p_{3/2}$ intensity increased by 21%. Given that the BE of Mn 2p increases with its oxidation state and its values in MnO, Mn_3O_4, Mn_2O_3, and MnO_2 are 641.0, 641.5, 641.9, and 642.4 eV, respectively,[13,23] the chemical valences of Mn in the Mn−Fe core and in MnO_2 shell are assigned to Mn(II) and Mn(IV), respectively.

The nitrogen adsorption−desorption isotherms of Mn−Fe and Mn−Fe/MnO_2 (Figure 4) can be assigned to Type II isotherms in IUPAC classification, implying that these particles are largely nonporous or macroporous. The Mn−Fe core had a pore volume of 0.36 cm^3/g and a SSA of 41.8 m^2/g. After coating, the pore volume of the obtained Mn−Fe/MnO_2 increased to 0.46 cm^3/g and its SSA increased to 113.3 m^2/g. This is in close agreement with the BET surface area of 100.5 m^2/g reported by Su et al.[14] and 117 m^2/g reported by Xu et al.[24] for MnO_2 particles. It also suggests that the magnetic Mn−

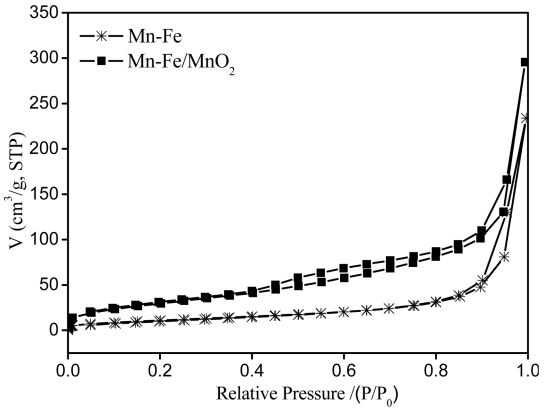

Figure 4. Nitrogen adsorption−desorption isotherms of Mn−Fe and Mn−Fe/MnO_2.

Fe core is almost completely coated by MnO_2 and the higher SSA of the Mn−Fe/MnO_2 particles is mainly due to the relatively high surface area of the MnO_2 shell.

The saturation magnetization (M_s) of Mn−Fe nanoparticles was 51.6 emu/g (Figure 5). This is slightly lower than that of

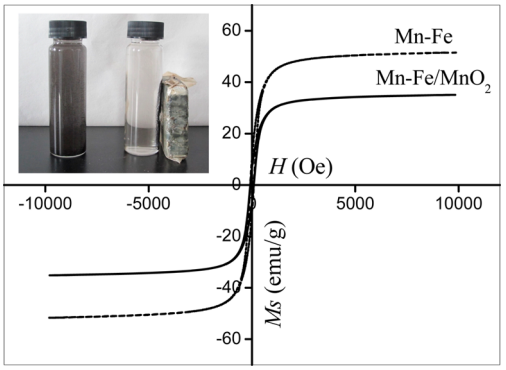

Figure 5. Magnetization curves of Mn−Fe and Mn−Fe/MnO_2.

Fe_3O_4 (57.4−68.1 emu/g) reported in the literature,[19,21,25] indicating that Mn^{2+} substitution for Fe^{2+} in Fe_3O_4 lattice may slightly decrease its M_s. The M_s of Mn−Fe/MnO_2 nanoparticles was 35.1 emu/g, very close to 36.2 emu/g for Fe_3O_4/SiO_2[19] and 33.5 emu/g for Fe_3O_4/MnO_2.[25] Although the nonmagnetic MnO_2 shell reduced the M_s of Mn−Fe/MnO_2 nanoparticles their complete separation was readily achieved by placing a magnet near the vessel containing the suspension (Figure 5). Furthermore, the nanoparticles rapidly redispersed when a magnetic field disappeared. Thus, Mn−Fe/MnO_2 has the potential to be used as a magnetic adsorbent to remove contaminants from water or wastewater.

3.2. Adsorption Capacities and Kinetics. *3.2.1. Adsorption Isotherms.* Mn−Fe/MnO_2 had a much higher Pb(II) adsorption capacity than magnetic core Mn−Fe (Figure 6). Furthermore, it was very effective in removing Pb(II) at a low equilibrium concentration, resulting in an adsorption capacity of 98.2, 139.9, and 209.6 mg/g at Pb(II) equilibrium concentrations of 0.6, 2.1, and 7.6 mg/L, respectively.

The data in Figure 6 were fitted into both the Langmuir model (eq 1) and Freundlich model (eq 2), as follows:

$$\frac{C_e}{q_e} = \frac{C_e}{q_m} + \frac{1}{q_m k_L} \quad (1)$$

dx.doi.org/10.1021/ie502967a | Ind. Eng. Chem. Res. 2014, 53, 18481−18488

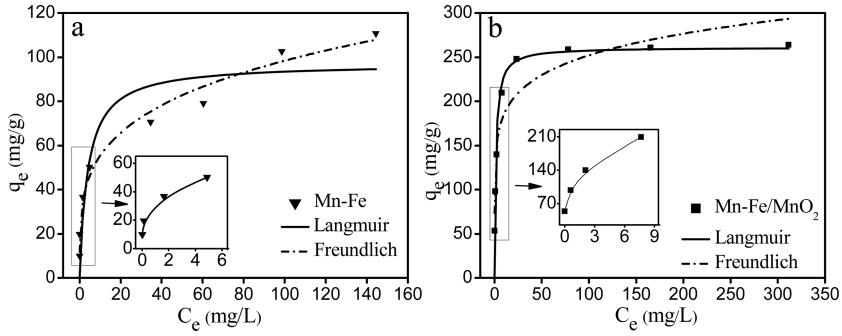

Figure 6. Adsorption isotherms for the Pb(II) by (a) Mn−Fe and (b) Mn−Fe/MnO_2 at pH = 5.0 ± 0.1, initial Pb(II) concentration = 5−350 mg/L, adsorbent dose = 0.500 g/L, contact time = 24 h, and T = 25 ± 1 °C.

Table 1. Langmuir and Freundlich Model Parameters for Pb(II) Adsorption on Mn−Fe and Mn−Fe/MnO_2

	Langmuir model			Freundlich model		
adsorbent	q_m (mg/g)	k_L (L/mg)	R^2	k_F (mg/g)	$1/n$	R^2
Mn−Fe	97.2	0.25	0.852	31.00	0.25	0.983
Mn−Fe/MnO_2	261.1	0.69	0.918	135.99	0.13	0.877

$$\log q_e = \frac{1}{n}\log C_e + \log k_F \quad (2)$$

where q_e (mg/g) is the amount of Pb(II) adsorbed on the adsorbent, C_e (mg/L) is the equilibrium Pb(II) concentration in solution phase, K_L (L/mg) is the equilibrium adsorption constant related to the affinity of binding sites, q_{max} is the maximum amount of the Pb(II) per unit weight of adsorbent for complete monolayer coverage, K_F is roughly an indicator of the adsorption capacity, and n is the heterogeneity factor which has a lower value for more heterogeneous surfaces.

As shown in Table 1, the adsorption data of the Mn−Fe core were better fitted into the Freundlich model (R^2 = 0.983) than the Langmuir model (R^2 = 0.852). This is possibly due to the heterogeneous nature of the adsorbent. In contrast, the Langmuir model better described the adsorption behavior of Pb(II) by Mn−Fe/MnO_2 than Freundlich model. This agrees with the assumption in the Langmuir model that adsorption occurs on a homogeneous surface, which would be the case after Mn−Fe core was completely coated with MnO_2 shell.

The maximal adsorption capacity calculated from the Langmuir model was 97.2 mg/g for Mn−Fe core and 261.1 mg/g for shell−core structured Mn−Fe/MnO_2.This suggests that the MnO_2 shell can endow the Mn−Fe/MnO_2 particles with a higher adsorption capacity for Pb(II) due to its large specific surface area and excellent surface characteristics. As shown in Table 2, the magnetic Mn−Fe core has a higher Pb(II) adsorption capacity than magnetic Fe_3O_4, $MnFe_2O_4$ and iron oxide nanoparticles. After the core was coated by MnO_2, the formed core−shell adsorbent inherited the excellent ability of MnO_2 for adsorbing Pb(II). Its maximal sorption capacity was nearly twice that of Fe_3O_4/MnO_2. Because Mn−Fe/MnO_2 remarkably outperforms many other metal oxide adsorbents it is a rather promising material for Pb(II) removal.

3.2.2. Adsorption Kinetics. Mn−Fe core and Mn−Fe/MnO_2 nanoparticles showed very different kinetics in Pb adsorption (Figure 7a). Mn−Fe/MnO_2 had a much faster initial adsorption stage than Mn−Fe core. Indeed, about 80% of the Pb(II) adsorption on Mn−Fe/MnO_2 occurred in the first 10 min. This was followed by a slow stage leading to the equilibrium.

Table 2. Maximum Pb(II) Adsorption Capacities of Different Adsorbents

adsorbent	Pb(II) concn range (mg/L)	Pb(II) adsorption capacity (mg/g)	ref
Fe_3O_4	5−350	69.8 (pH 5.0)	21
$MnFe_2O_4$	10−250	69.1 (pH 6.0)	26
iron oxide nanoparticles	10−800	35.8(pH 5.5)	27
Mn(II)-bearing Fe_3O_4	5−160	97.2 (pH 5.0)	present study
hydrous manganese dioxide	12.59−53.96	352.5 (pH 4.0)	12
hydrous manganese dioxide		327.0 (pH 3.5)	14
activated alumina	3−300	80.3(pH 5.0)	28
Fe_3O_4/SiO_2−NH_2	10−100	76.6 (pH 6.2)	19
Fe, Mg oxides coatings onto bentonite	30−120	95.9 (pH 4.0)	7
Fe_3O_4/MnO_2	5−350	142.0 (pH 5.0)	21
Mn−Fe/MnO_2	5−350	261.1 (pH 5.0)	present study

To further characterize the adsorption process, data obtained from batch experiments were fitted into the pseudo-first-order (eq 3), pseudo-second-order (eq 4), and intraparticle diffusion (eq 5) adsorption models, as follows:

$$\log(q_e - q_t) = \log q_e - \frac{k_1 t}{2.303} \quad (3)$$

$$\frac{t}{q_t} = \frac{1}{k_2 q_e^2} + \frac{t}{q_e} \quad (4)$$

$$q_e = k_p t^{0.5} + C \quad (5)$$

where q_e and q_t are adsorption capacities (mg/g) at equilibrium and at time t (min), respectively; k_1 (min^{-1}), k_2 (mg/g·min), and k_p (mg/g·$min^{0.5}$) are the related adsorption rate constants; C (mg/g) is a constant gained from the intercept in the plot of q_t against $t^{0.5}$.

The linear forms of the data fitting into the three models are shown in Figure 7b−d, and the obtained adsorption rate constants are given in Table 3. For both Mn−Fe and Mn−Fe/

dx.doi.org/10.1021/ie502967a | Ind. Eng. Chem. Res. 2014, 53, 18481−18488

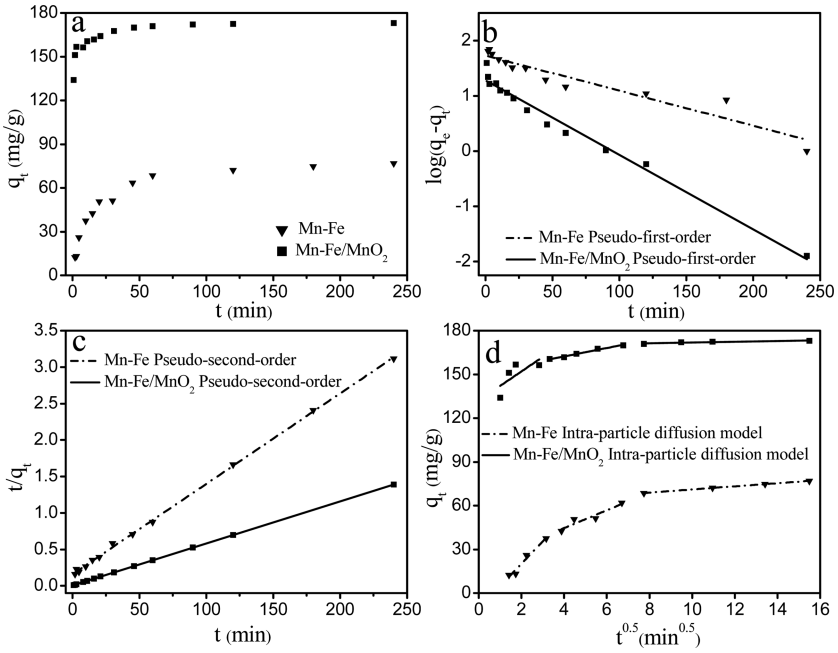

Figure 7. Kinetics of Pb(II) adsorption onto Mn−Fe and Mn−Fe/MnO_2 at pH = 5.0 ± 0.1, initial Pb(II) concentration = 100 mg/L, adsorbent dose = 0.500 g/L, and T = 25 ± 1 °C: (a) adsorption capacity vs contact time, (b) the linear form of the pseudo-first-order model, (c) the linear form of the pseudo-second-order model, and (d) the linear form of the intraparticle diffusion model.

Table 3. Kinetic Parameters for Pb Adsorption on Mn−Fe and Mn−Fe/MnO_2

	pseudo-first-order model			pseudo-second-order model			intraparticle diffusion model		
adsorbent	q_e (mg/g)	k_1 (min^{-1})	R^2	q_e (mg/g)	k_2 (mg/g·min)	R^2	q_e (mg/g)	k_p (mg/g·$min^{0.5}$)	R^2
Fe−Mn	71.85	0.06	0.958	80.07	0.001	0.989	76.90	6.11	0.858
Fe−Mn/MnO_2	165.7	1.53	0.673	169.1	0.022	0.880	173.2	2.89	0.976

MnO_2, the R^2 values suggest that pseudo-second-order model suits better than the pseudo-first-order model. As for Mn−Fe/MnO_2, the intraparticle diffusion model describes the adsorption process best, implying that intraparticle diffusion is the rate-limiting step for the removal of Pb(II) by the adsorbents.

The adsorption process may be divided into three stages (Figure 7d). The first (0−10 min) was the external surface (or instantaneous) adsorption stage. This might be attributed to the large quantity of active adsorptive sites on the surfaces of Mn−Fe/MnO_2, where Pb(II) quickly moved through the solid/solution interface under concentration gradient. The second stage (10 min −60 min) was a gradual process during which intraparticle diffusion started to limit the rate of adsorption. The third one (60 min−240 min) was the equilibrium stage, during which the internal adsorptive sites were gradually saturated.

3.2.3. Effect of pH, Ionic Strength, And Cations on Pb(II) Adsorption. pH played an important role in the adsorption process, and Pb(II) removal efficiency increased with pH (Figure 8). Such a pH effect has been reported for Pb(II) adsorption onto iron and manganese oxides.[7,13,19,26] At pH < 3.0, Pb(II) was hardly adsorbed on the surface of Mn−Fe/MnO_2 because the point of zero charge of the MnO_2 was reported at pH 2.0−3.0.[29,30] At pH > 3.0 deprotonation increased the negative charge on the surface of Mn−Fe/MnO_2, thus enhancing the electrostatic attraction between the adsorbent and Pb(II) and increasing adsorption capacity dramatically. Besides influencing the surface charge and the dissociation of functional groups on the surface of adsorbent, pH also determines the chemical species of Pb in solution. Pb^{2+} is the dominant species at low pH values. It hydrolyzes to form $Pb(OH)^+$ and $Pb(OH)_2$ with the increase in pH. The precipitation constant of $Pb(OH)_2$ is 1.2×10^{-15}, which means that precipitation plays a key role at pH > 7.8. A pH of 5.0 ± 0.1 was chosen in this study for Pb(II) adsorption to ensure that no hydroxide precipitation was formed and the large adsorption capacity of the Mn−Fe/MnO_2 was not due to precipitation.

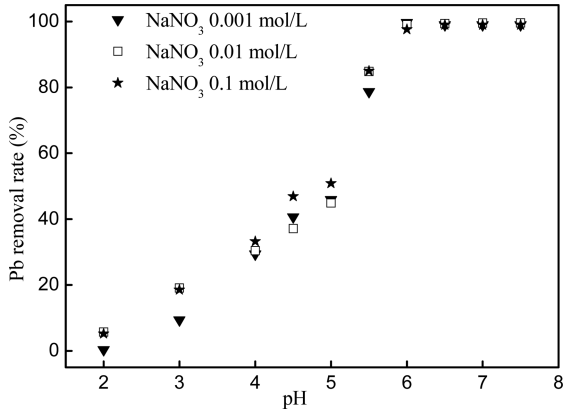

Figure 8. Effect of pH and ionic strength on Pb(II) adsorption by Mn−Fe/MnO_2. Initial Pb(II) concentration = 100 mg/L, adsorbent dose = 0.500 g/L, and T = 25 ± 1 °C.

dx.doi.org/10.1021/ie502967a | *Ind. Eng. Chem. Res.* 2014, 53, 18481−18488

The increase in ionic strength from 0.001 to 0.1 mol/L slightly enhanced Pb adsorption in the pH range of 2.5−5.5. It had no effect on Pb adsorption at pH > 6.5. Outer-sphere surface complexation is strongly sensitive to ionic strength variation because the background electrolyte ions are placed in the same plane as Pb^{2+} in outer-sphere surface complexes.[7] Conversely, adsorption by inner-sphere complex either shows little sensitivity to ionic strength or responds to a higher ionic strength with a greater adsorption.[31] Therefore, it might be deduced that Pb(II) formed inner-sphere complexes on the surface of Mn−Fe/MnO_2. Similar conclusions were made in the literature on the removal of Pb(II) by hydrous manganese dioxide[12] and manganese oxide-coated bentonite.[32]

Ca(II), Mg(II), and Zn(II), as coexisting cations, did not affect Pb(II) adsorption (Figure 9), whereas a slight reduction in Pb(II) adsorption occurred when the concentration of coexisting Cu(II) (2.5 mM) was about 1 order of magnitude higher than Pb(II) concentration. This preferable adsorption toward Pb(II) may be attributable to the formation of an inner-sphere complex,[13,14] in which strong covalent bonds were formed between Pb(II) and the surface functional groups of the Mn−Fe/MnO_2. Its high selectivity for Pb(II) determines the potential use of Mn−Fe/MnO_2 as a preferable adsorbent of Pb(II), even in the presence of competing cations at high concentrations.

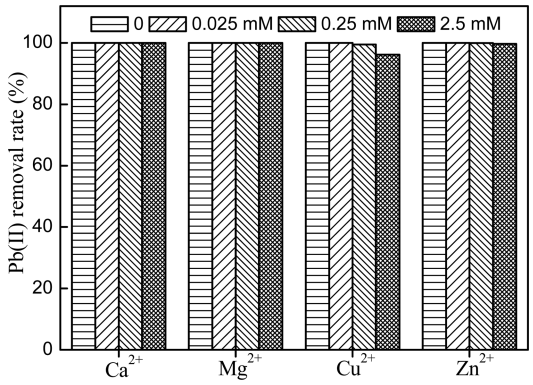

Figure 9. Effect of coexisting cations on Pb(II) adsorption by Mn−Fe/MnO_2. Initial Pb(II) concentration = 50 mg/L, adsorbent dose = 0.500 g/L, contact time = 24 h, pH = 5.0 ± 0.1, and T = 25 ± 1 °C

3.3. XPS Evidence for Inner-sphere Complexation. The analysis of the compositions and speciation of the elements on the surface of Mn−Fe/MnO_2 before and after Pb(II) load provides an insight on adsorption process. A new peak of Pb 4f appeared in the spectrum of Mn−Fe/MnO_2 (Figure 10a) after its reaction with Pb(II), confirming its adsorption. This core level spectrum of Pb 4f (Figure 10b) was assigned to Pb $4f_{7/2}$ (138.1 eV) and Pb $4f_{5/2}$ (143.0 eV). The chemical valence of Pb adsorbed on Mn−Fe/MnO_2 was determined divalent thereafter.[12,26]

The core level spectra of O 1s (Figure 10c,d) comprises three overlapped peaks of lattice oxygen (O^{2-}), hydroxyl (OH^-), and adsorbed water (H_2O). The peak with BE of 529.71 eV, being the characteristic of oxygen in the Mn−Fe/MnO_2, was assigned to O^{2-}. The peak at 530.90 eV was assigned to OH^- on the surface of Mn−Fe/MnO_2, which is a key contributor to Pb(II) adsorption by metal oxides.[26,33] The ratio of the integral area of the O^{2-} to the total oxygen increased from 60.22% to 62.65% after Pb(II) adsorption. Meanwhile, the surface OH^- group content decreased from 31.12% to 26.70%.

The above results and discussion lead to the conclusion that Pb(II) uptake by Mn−Fe/MnO_2 is mainly achieved through the formation of a surface complex between hydroxyl groups and Pb(II), as shown in eq 6.

$$2M{-}OH + Pb^{2+} \rightarrow (M{-}O)_2Pb + 2H^+ \quad (6)$$

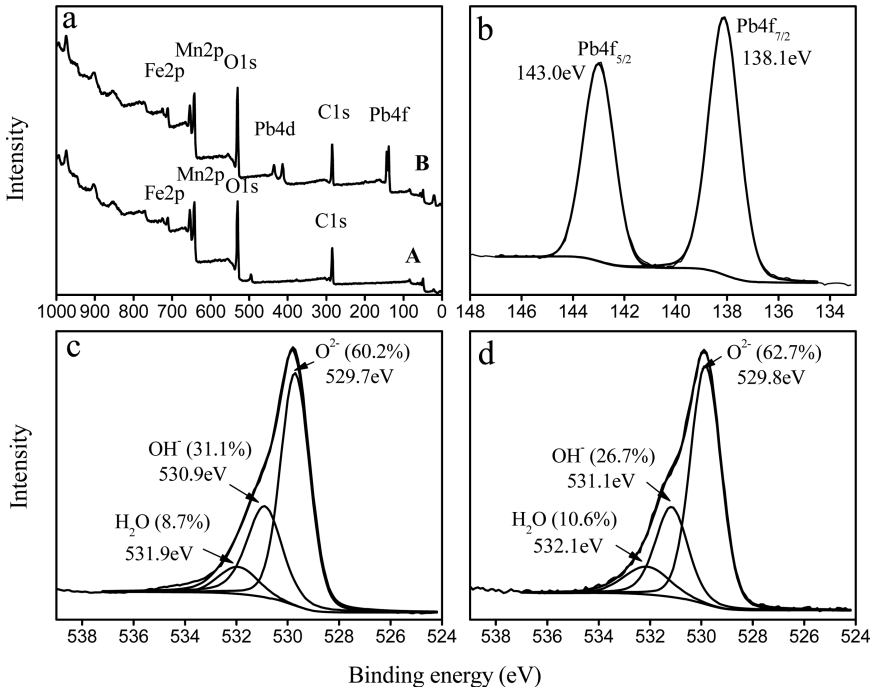

Figure 10. XPS spectra of Mn−Fe/MnO_2: (a) wide-scan spectra (A as prepared and B after reaction with Pb); (b) detailed spectra of Pb $4f_{7/2}$ after Pb(II) adsorption; (c) O 1s spectra before Pb(II) adsorption; and (d) O 1s spectra after Pb(II) adsorption.

dx.doi.org/10.1021/ie502967a | Ind. Eng. Chem. Res. 2014, 53, 18481−18488

Obviously, an increase in pH would help consume H^+, thus enhancing Pb adsorption.

3.4. Adsorbent Reusability. Reusability is an important factor for consideration in developing practical applications of adsorbents. Figure 11 shows the ability of the synthetic Mn−

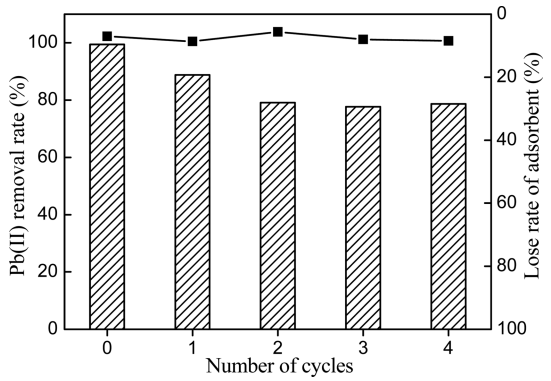

Figure 11. Pb(II) adsorption on regenerated Mn−Fe/MnO_2 (bars) and its loss rate of adsorbent with four adsorption−regeneration cycles (squares and line). Adsorption condition: initial Pb(II) concentration = 100 mg/L, adsorbent dose = 1.00 g/L, contact time = 8 h, pH = 5.0 ± 0.1, and T = 25 ± 1 °C. Desorption condition: regenerant 100 mL 0.1 M HCl, contact time = 1 h, and T = 25 ± 1 °C.

Fe/MnO_2 nanoparticles to be regenerated for reuse. At their first encounter Pb(II) adsorption onto Mn−Fe/MnO_2 was extremely strong, with a removal rate close to 100%. As the number of regeneration cycles increased, the removal rate decreased. This may be due to the incomplete release of adsorbed Pb(II) in the last regeneration and the partial loss of the adsorbent itself (5.6−8.6%) during the multiregeneration processes. Nevertheless, the decrease and loss were not significant. Even after four cycles, 80% of the original adsorption efficiency was retained. Its facile synthesis, easy regeneration, high adsorption efficiency after repeated uses, and inexpensiveness determine that magnetic nanoparticles of Mn−Fe/MnO_2 have the potential for practical use in environmental remediation.

4. CONCLUSIONS

A novel core−shell structured adsorbent (Mn−Fe/MnO_2) with Mn(II)-bearing Fe_3O_4 as magnetic core and MnO_2 as shell was successfully synthesized using a coprecipitation method. It inherited the high Pb(II) adsorption ability of the MnO_2 shell. Its adsorption process was pH-dependent, insensitive to competing cations, and dominated by the inner-sphere complexation. With a maximal adsorption capacity for Pb(II) of 261.1 mg/g at pH 5.0, it outperforms many other metal oxide adsorbents. Furthermore, the adsorbent can be easily separated from aqueous solutions using a magnetic technique, readily regenerated with acid washing, and reused with a good performance. These desirable properties make Mn−Fe/MnO_2 a promising adsorbent for use in the removal of Pb(II) from water or wastewater.

AUTHOR INFORMATION

Corresponding Author

* E-mail: gszhang@yic.ac.cn. Tel./Fax: +86-535-2109139.

Notes

The authors declare no competing financial interest.

ACKNOWLEDGMENTS

The authors acknowledge the financial support from National Natural Science Foundation of China (51178453), the Key Research Program of the Chinese Academy of Sciences (KZZD-EW-14), and the Science and Technology Project of Yantai (2014ZH087).

REFERENCES

(1) Fu, F.; Wang, Q. Removal of heavy metal ions from wastewaters: A review. *J. Environ. Manage.* **2011**, *92*, 407.
(2) Li, Y.; Wang, J. D.; Wang, X. J.; Wang, J. F. Adsorption−Desorption of Cd(II) and Pb(II) on Ca-Montmorillonite. *Ind. Eng. Chem. Res.* **2012**, *51*, 6520.
(3) World Health Organization. *Guidelines for Drinking-Water Quality*, 4th ed.; WHO: Geneva, Switzerland, 2011.
(4) Environmental Protection Agency. *Lead and Copper Rule: A Quick Reference Guide for Schools and Child Care Facilities That Are Regulated under the Safe Drinking Water Act*. Office of Water, EPA: Washington, DC, 2005.
(5) Qu, J. Research progress of novel adsorption processes in water purification: A review. *J. Environ. Sci.* **2008**, *20*, 1.
(6) Khan, N. A.; Hasan, Z.; Jhung, S. H. Adsorptive removal of hazardous materials using metal-organic frameworks (MOFs): A review. *J. Hazard. Mater.* **2013**, *244−245*, 444.
(7) Ranđelović, M.; Purenović, M.; Zarubica, A.; Purenović, J.; Matović, B.; Momčilović, M. Synthesis of composite by application of mixed Fe, Mg (hydr)oxides coatings onto bentonite—A use for the removal of Pb(II) from water. *J. Hazard. Mater.* **2012**, *199−200*, 367.
(8) Hua, M.; Zhang, S.; Pan, B.; Zhang, W.; Lv, L.; Zhang, Q. Heavy metal removal from water/wastewater by nanosized metal oxides: A review. *J. Hazard. Mater.* **2012**, *211−212*, 317.
(9) Xu, P.; Zeng, G. M.; Huang, D. L.; Feng, C. L.; Hu, S.; Zhao, M. H.; Lai, C.; Wei, Z.; Huang, C.; Xie, G. X.; Liu, Z. F. Use of iron oxide nanomaterials in wastewater treatment: A review. *Sci. Total Environ.* **2012**, *424*, 1.
(10) Ouvrard, S.; Simonnot, M. O.; Donato, P.; de Sardin, M. Diffusion-controlled adsorption of arsenate on a natural manganese oxide. *Ind. Eng. Chem. Res.* **2002**, *41*, 6194.
(11) Rout, K.; Mohapatra, M.; Anand, S. A critical analysis of cation adsorption from single and binary solutions on low surface area β-MnO_2. *Appl. Surf. Sci.* **2013**, *270*, 205.
(12) Xu, M.; Wang, H.; Lei, D.; Qu, D.; Zhai, Y.; Wang, Y. Removal of Pb(II) from aqueous solution by hydrous manganese dioxide: Adsorption behavior and mechanism. *J. Environ. Sci.* **2013**, *25*, 479.
(13) Qin, Q.; Wang, Q.; Fu, D.; Ma, J. An efficient approach for Pb(II) and Cd(II) removal using manganese dioxide formed in situ. *Chem. Eng. J.* **2011**, *172*, 68.
(14) Su, Q.; Pan, B.; Wan, S.; Zhang, W.; Lv, L. Use of hydrous manganese dioxide as a potential sorbent for selective removal of lead, cadmium, and zinc ions from water. *J. Colloid Interface Sci.* **2010**, *349*, 607.
(15) Wan, S.; Zhao, X.; Lv, L.; Su, Q.; Gu, H.; Pan, B.; Zhang, W.; Lin, Z.; Luan, J. Selective adsorption of Cd(II) and Zn(II) ions by nano-hydrous manganese dioxide (HMO)-encapsulated cation exchanger. *Ind. Eng. Chem. Res.* **2010**, *49*, 7574.
(16) Ambashta, R. D.; Sillanpää, M. Water purification using magnetic assistance: A review. *J. Hazard. Mater.* **2010**, *180*, 38.
(17) Broomberg, J.; Célinas, S.; Finch, J. A.; Xu, Z. Review of magnetic carrier technologies for metal ion removal. *Magn. Electr. Sep.* **1999**, *9*, 169.
(18) Tang, S. C. N.; Lo, I. M. C. Magnetic nanoparticles: Essential factors for sustainable environmental applications. *Water Res.* **2013**, *47*, 2613.
(19) Wang, J.; Zheng, S.; Shao, Y.; Liu, J.; Xu, Z.; Zhu, D. Amino-functionalized Fe_3O_4/SiO_2 core−shell magnetic nanomaterial as a novel adsorbent for aqueous heavy metals removal. *J. Colloid Interface Sci.* **2010**, *349*, 293.

(20) Warner, C. L.; Chouyyok, W.; Mackie, K. E.; Neiner, D.; Saraf, L. V.; Droubay, T. C.; Warner, M. G.; Addleman, R. S. Manganese doping of magnetic iron oxide nanoparticles: Tailoring surface reactivity for a regenerable heavy metal sorbent. *Langmuir* **2012**, *28*, 3931.
(21) Zhang, X. L.; Chen, J.; Han, J. L.; Zhang, G. S. Preparation and evaluation of shell-core structured Fe_3O_4/MnO_2 magnetic adsorbent for Pb(II) removal from aqueous solutions. *Acta Sci. Circumstant.* **2013**, *33*, 2730.
(22) Kodama, T.; Ookubo, M.; Miura, S.; Kitayama, Y. Synthesis and characterization of ultrafine Mn(II)-bearing ferrite of type $Mn_xFe_{3-x}O_4$ by coprecipitation. *Mater. Res. Bull.* **1996**, *31*, 1501.
(23) Katsoyiannis, I. A.; Zouboulis, A. I. Biological treatment of Mn(II) and Fe(II) containing groundwater: kinetic considerations and product characterization. *Water Res.* **2004**, *38*, 1922.
(24) Xu, W.; Wang, H.; Liu, R.; Zhao, X.; Qu, J. The mechanism of antimony (III) removal and its reactions on the surfaces of Fe−Mn binary oxide. *J. Colloid Interface Sci.* **2011**, *363*, 320.
(25) Shu, Z.; Wang, S. Synthesis and characterization of magnetic nanosized Fe_3O_4/MnO_2 composite particles. *J. Nanomater.* **2009**, doi:10.1155/2009/340217, URL://WOS:000261577000001.
(26) Ren, Y.; Li, N.; Feng, J.; Luan, T.; Wen, Q.; Li, Z.; Zhang, M. Adsorption of Pb(II) and Cu(II) from aqueous solution on magnetic porous ferrospinel $MnFe_2O_4$. *J. Colloid Interface Sci.* **2012**, *367*, 415.
(27) Nassar, N. N. Rapid removal and recovery of Pb(II) from wastewater by magnetic nanoadsorbents. *J. Hazard. Mater.* **2010**, *184*, 538.
(28) Naiya, T. K.; Bhattacharya, A. K.; Das, S. K. Adsorption of Cd(II) and Pb(II) from aqueous solutions on activated alumina. *J. Colloid Interface Sci.* **2009**, *333*, 14.
(29) Zhang, G.; Liu, H.; Qu, J.; Jefferson, W. Arsenate uptake and arsenite simultaneous sorption and oxidation by Fe−Mn binary oxides: Influence of Mn/Fe ratio, pH, Ca^{2+}, and humic acid. *J. Colloid Interface Sci.* **2012**, *366*, 141.
(30) Kanungo, S. B.; Mahapatra, D. M. Interfacial properties of some hydrous manganese dioxides in 1−1 electrolyte solution. *J. Colloid Interface Sci.* **1989**, *131*, 103.
(31) Zhang, G.; Liu, H.; Liu, R.; Qu, J. Adsorption behavior and mechanism of arsenate at Fe−Mn binary oxide/water interface. *J. Hazard. Mater.* **2009**, *168*, 820.
(32) Eren, E.; Afsin, B.; Onal, Y. Removal of lead ions by acid activated and manganese oxide-coated bentonite. *J. Hazard. Mater.* **2009**, *161*, 677.
(33) Zhang, G. S.; Qu, J. H.; Liu, H. J.; Liu, R. P.; Li, G. T. Removal mechanism of As(III) by a novel Fe−Mn binary oxide adsorbent: Oxidation and sorption. *Environ. Sci. Technol.* **2007**, *41*, 4613.